

Article

Three-Dimensional Quantification and Visualization of Leaf Chlorophyll Content in Poplar Saplings under Drought Using SFM-MVS

Qifei Tian ¹, Huichun Zhang ^{1,2,*}, Liming Bian ³, Lei Zhou ¹ and Yufeng Ge ^{4,5}

¹ College of Mechanical and Electronic Engineering, Nanjing Forestry University, Nanjing 210037, China

² Jiangsu Co-Innovation Center of Efficient Processing and Utilization of Forest Resources, Nanjing Forestry University, Nanjing 210037, China

³ College of Forestry, Nanjing Forestry University, Nanjing 210037, China

⁴ Department of Biological Systems Engineering, University of Nebraska-Lincoln, Lincoln, NE 68588, USA

⁵ Center for Plant Science Innovation, University of Nebraska-Lincoln, Lincoln, NE 68588, USA

* Correspondence: njzhanghc@hotmail.com; Tel.: +86-025-85427765

Abstract: As global temperatures warm, drought reduces plant yields and is one of the most serious abiotic stresses causing plant losses. The early identification of plant drought is of great significance for making improvement decisions in advance. Chlorophyll is closely related to plant photosynthesis and nutritional status. By tracking the changes in chlorophyll between plant strains, we can identify the impact of drought on a plant's physiological status, efficiently adjust the plant's ecosystem adaptability, and achieve optimization of planting management strategies and resource utilization efficiency. Plant three-dimensional reconstruction and three-dimensional character description are current research hot spots in the development of phenomics, which can three-dimensionally reveal the impact of drought on plant structure and physiological phenotypes. This article obtains visible light multi-view images of four poplar varieties before and after drought. Machine learning algorithms were used to establish the regression models between color vegetation indices and chlorophyll content. The model, based on the partial least squares regression (PLSR), reached the best performance, with an R^2 of 0.711. The SFM-MVS algorithm was used to reconstruct the plant's three-dimensional point cloud and perform color correction, point cloud noise reduction, and morphological calibration. The trained PLSR chlorophyll prediction model was combined with the point cloud color information, and the point cloud color was re-rendered to achieve three-dimensional digitization of plant chlorophyll content. Experimental research found that under natural growth conditions, the chlorophyll content of poplar trees showed a gradient distribution state with gradually increasing values from top to bottom; after being given a short period of mild drought stress, the chlorophyll content accumulated. Compared with the value before stress, it has improved, but no longer presents a gradient distribution state. At the same time, after severe drought stress, the chlorophyll value decreased as a whole, and the lower leaves began to turn yellow, wilt and fall off; when the stress intensity was consistent with the duration, the effect of drought on the chlorophyll value was $895 < SY-1 < 110 < 3804$. This research provides an effective tool for in-depth understanding of the mechanisms and physiological responses of plants to environmental stress. It is of great significance for improving agricultural and forestry production and protecting the ecological environment. It also provides decision-making for solving plant drought problems caused by global climate change.



Citation: Tian, Q.; Zhang, H.; Bian, L.; Zhou, L.; Ge, Y. Three-Dimensional Quantification and Visualization of Leaf Chlorophyll Content in Poplar Saplings under Drought Using SFM-MVS. *Forests* **2024**, *15*, 20. <https://doi.org/10.3390/f15010020>

Academic Editor: Eric Casella

Received: 17 November 2023

Revised: 14 December 2023

Accepted: 18 December 2023

Published: 20 December 2023



Copyright: © 2023 by the authors. Licensee MDPI, Basel, Switzerland. This article is an open access article distributed under the terms and conditions of the Creative Commons Attribution (CC BY) license (<https://creativecommons.org/licenses/by/4.0/>).

Keywords: plant phenotyping; point cloud; structure from motion-multi-view stereo; chlorophyll; three-dimensional visualization; machine learning

1. Introduction

Drought is recognized as the most detrimental environmental stress that adversely affects tree growth such as blocked photosynthesis and, consequently, forest productiv-

ity, playing a pivotal role in shaping the geographic distribution of tree species [1–3]. The impact of drought stress induces a diverse range of reactions in plants, which vary based on genotype, plant size, growth stage, and the intensity and timing of the drought. Understanding tree responses and tolerance to drought stress involves complex biological processes that can be elucidated more comprehensively through the use of emerging imaging sensors and phenotyping technologies [4].

Chlorophyll affects all essential physiological and developmental processes of plants, and it is known as a probe for photosynthesis, metabolism and plant vitality [5]. The biological mechanism response of plant chlorophyll to drought stress can be explained as: the stomatal conductance of leaves is reduced, the synthesis of chlorophyll is blocked, and the decomposition rate of chlorophyll is accelerated, thereby hindering leaf photosynthesis and causing large fluctuations in chlorophyll content [6]. Therefore, monitoring the dynamic changes of plant chlorophyll can provide a theoretical reference for identifying early drought in plants. It is also of great significance for optimizing water management strategies and accelerating the breeding of drought-resistant forest trees [7].

In the early days, chlorophyll content was mainly measured using laboratory physical and chemical analysis methods such as acetone extraction. The measurement process had defects such as high cost, low efficiency, and was destructive and unrecoverable [8]. The traditional spectrophotometric method used to measure the chlorophyll content of plant leaves has the advantages of high measurement accuracy and good repeatability, but the measurement process is time-consuming. A portable rapid chlorophyll detector can be used in situ measurement. However, the actual measurement area of the detector is very small (for example, the measurement area of SPAD-502 is only 2×3 mm). It requires measuring and averaging the values after multi-point sampling and the measurement results are easily affected by the thickness of the blade [9].

Recently, non-destructive analysis and rapid technology based on images and spectra has been developed to detect the chlorophyll content. The principle of these methods is that by obtaining an average spectrum, average color, or single point detection of the plant surface, only the chlorophyll content of a single sampling point or the overall average can be predicted [10]. The distribution among various plant organs is still unclear. Some scholars use methods, such as chlorophyll fluorescence and spectral reflectance, to visualize the chlorophyll content of plant canopy leaves, but most can only achieve a two-dimensional scale, and integrated fluorescence analyzers and spectral sensors also have high requirements for the imaging environment and high price, thus limiting its application to a wide range [11]. At the same time, due to the limitation of data dimension and spatial resolution, the image and spectral information from an overhead view or a single perspective can only reflect the phenotypic information of plants projected at a certain static angle, and it is difficult to perceive the stereoscopic changes of plant phenotype between different organs caused by physiological stress, water, and fertilizer deficiency and other reasons. By analyzing the vertical distribution of plant chlorophyll at the three-dimensional level, we can understand the adaptability of different plant species in different ecosystems, reveal the patterns of photosynthesis and carbon fixation, and evaluate the growth state and health status of plants [12–14].

With the continuous iterative updates of optical sensors, three-dimensional point cloud data of plants are obtained through Lidar and RGB-D to reflect the true growth status of plants and obtain morphological characteristics, it has been widely used and developed in forestry phenotypic research [15–17]. However, compared with their research applications at short range and single plant scale, the structure from motion-multi view stereo (SFM-MVS) technology is more widely used and less expensive. In addition, SFM-MVS can provide more detailed plant surface texture and color information, ensuring the integrity of the plant structure to a higher level [18,19].

Poplar (*Populus* spp.) is an important fast-growing and high-yield tree species in the world, with a wide range of planted areas, which make significant contributions to the world's ecosystem services, such as soil and water conservation and carbon sequestra-

tion [20]. However, drought has resulted in extremely severe yield reductions and losses in large areas of poplar trees [21]. Monitoring the distribution and changes of poplar chlorophyll content through multidisciplinary integration, identifying the stress level of poplar trees as early as possible, and making artificial water management improvements in advance have been promoted and applied at the two-dimensional image scale, but most methods can only analyze the plants' overall condition, and the lack of detailed information limits the performance of plant growth status determination [22,23]. By combining three-dimensional technology and machine learning methods to evaluate the spatial distribution differences and changing responses of chlorophyll content of different varieties or strains under drought stress, it provides a technical reference for cultivating high-quality drought-resistant genotype poplar varieties and maximizing economic benefits and ecological value [24].

The objective of this study is to: (i) develop and verify a method based on image analysis for non-destructive determination of chlorophyll content in poplar seedlings, (ii) use SFM-MVS combined with a chlorophyll regression model to solve the problem of chlorophyll content in poplar three-dimensional model, (iii) analyze the effects of genotype differences and differences in drought stress levels on the distribution of poplar chlorophyll content among organs under multiple growth periods.

2. Materials and Methods

2.1. Experiment Material

Four species of poplar seedlings were selected in the experiment, which had great differences in morphological structure and drought tolerance, including the drought-tolerant varieties *Siyang-1 poplar* (SY-1) and *3804 poplar* (3804), the hydrophilous varieties *895 poplar* (895) and *110 poplar* (*Populus cathayana* Rehder). In total, 48 plants of each variety were cultured in 3 water treatment groups. A total of 192 plants were planted in the experiment. All plant cuttings were cultivated in pots with a capacity of 5.8 L and placed outdoors to grow naturally.

2.2. Experimental Design

The planting time of poplar seedlings is unified (11 March 2023). Data were collected after 70 days of normal cultivation (21 May 2023). At this time, the average height of poplar varieties was distributed in the range of 40–50 cm, and the plants had certain drought resistance. For each poplar variety, 8 plants with uniform growth in three water treatment groups were selected as samples for multi-view image collection. Table 1 below summarizes the experiment. Before initiating drought treatment, data were collected from all samples every 7 days, totaling 96 samples, and image data were collected four times. Following the fourth data collection, a 15-day drought treatment commenced, categorized into three levels: control check group (CK), mild drought group (MD), and severe drought group (SD). Each treatment group comprised 32 samples.

Table 1. General profile of the experiment.

	Before Drought Treatment	After Drought Treatment		
Image acquisition times	4		1	
Experiment sample size	96	Control check 32	Mild drought 32	Severe drought 32
Experiment interval date (days)	7		15	

Drought has caused great differences in the growth rate, color, and other phenotypes of poplar plants to verify the reliability of this article's multi-view visualization of chlorophyll three-dimensional distribution and explore the growth habits and drought resistance of different poplar varieties. After each image collection, the handheld chlorophyll meter SPAD-502 (SPAD-502 Plus; Minolta Camera Co. Osaka, Japan) was used to measure the

chlorophyll content of the three upper leaves and the three lower leaves of the poplar plant after each image collection, respectively, then the average value was calculated as a reference for the true value of the chlorophyll content of the poplar leaves.

2.3. Multi-View Image Acquisition

Visible light cameras are currently mature imaging sensors and have been widely used in various research fields of plant phenotypes. In this study, all poplar multi-view sub-images of SFM-MVS were captured by a camera, a tripod, a rotating disk, and a black absorbent cloth under uniform lighting and windless conditions, as shown in Figure 1. Image (a) on the left displays all project equipment, while image (b) on the right illustrates on-site activities.

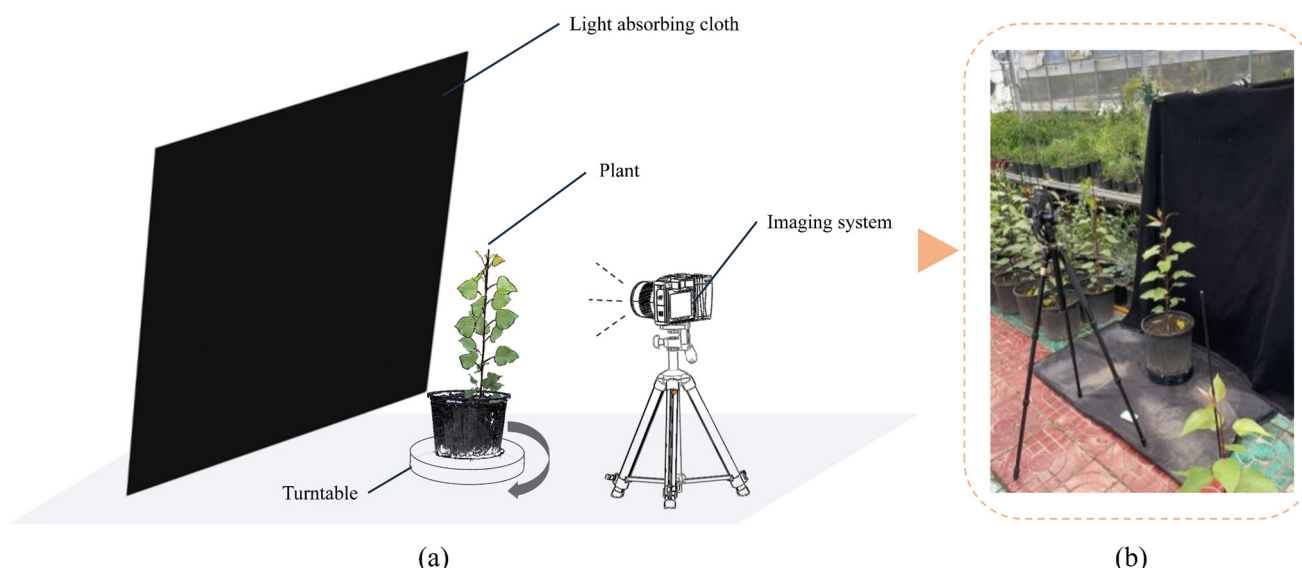


Figure 1. Schematic diagram of multi-view image acquisition. Illustration: (a) Image acquisition system diagram; (b) On-site work demonstration.

The plants were placed in the center of the rotating disc for uniform rotation. In order to keep the leaves as still as possible in the course of the rotating process, the rotation speed was set at $6\text{--}8^\circ/\text{s}$, and the photo taking mode was set at intervals of 2 s, the number of photos taken for each poplar tree was 30, the camera model used and all imaging parameter settings are listed in Table 2.

Table 2. Camera models and parameters for acquiring multi-view images.

Specific Parameters (Symbol)	Camera Model Nikon Z5	
	Numerical Value	Unit
Shutter speed (S)	1/320	Seconds (s)
Aperture (A)	10	Dimensionless
Speed (ISO)	100	Dimensionless
Imaging focal length (f)	35	Millimeter (mm)
Image storage format (F)	JPG	Dimensionless
Picture size (P)	4016 × 6016	Pixels per inch (PPI)
Total rotation Angle (θ)	400	Degree ($^\circ$)

In order to improve the efficiency and accuracy of using SFM-MVS technology to reconstruct poplar point clouds, the imaging distance, focal length, and angle of the camera were basically kept consistent when collecting images. Considering that the lighting environment and imaging background will have a great impact on image quality and color, the checkerboard pattern and Color Checker 24-color standard color card were taken before

data acquisition to correct image distortion, white balance and color. A single test collected 96 sample data images, and the five tests totaled 480 poplar samples and 14,400 pictures.

3. Methods and Materials

3.1. Image Pre-Processing

The original plant images obtained in the experiment have a high resolution and large storage capacity, but most of the information is redundant, which will reduce the efficiency and accuracy of plant 3D point cloud reconstruction. In order to eliminate irrelevant information, such as background and ground, this study plans to perform image pre-processing as shown in Figure 2 below, including: (a) Image correction, where (1) is a schematic representation of the original image; (2) signifies white balance, color, and distortion correction; with (3) portraying the image post-correction. Additionally, (b) involves image segmentation, with (4) denoting excess green calculation; (5) representing the threshold segmentation diagram; and (6) illustrating the image opening operation. Finally, the corrected image (3) is utilized to overlay the noise-reduced image (6) mask, resulting in the mask image (7). The size of an individual image in this process ranges from 0.7 to 0.9 MB.

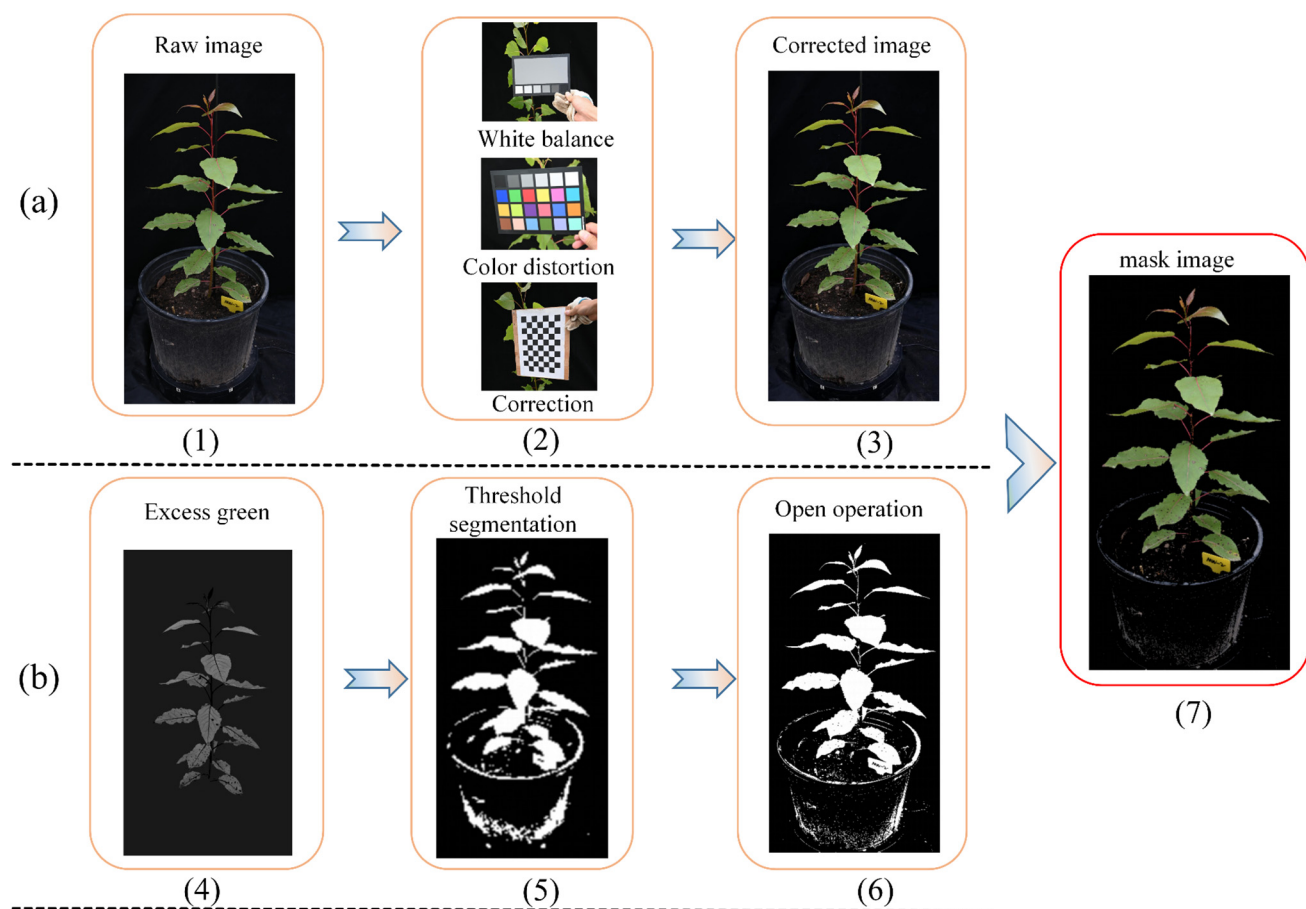


Figure 2. Image pre-processing before 3D reconstruction. Illustration: (a,b) represent image correction and denoising, respectively. Where, (1) raw image, (2) image white balance, color and distortion correction, (3) corrected image, (4) excess green calculation, (5) threshold segmentation, (6) image opening operation, (7) processed image.

Among them, in the process of image white balance and color correction, the Color Checker 24-color standard color card image was used to match the feature points with the color card image, including plants taken during the test, and the coordinate position of the color card in the test image was detected. After correcting the position of the color card

through perspective transformation, the actual size of the R, G, and B values of each color patch are calculated. The standard R, G, and B values of the same color card are used to generate a correction matrix. All test images are traversed and the mapping relationship is used to complete the color correction and white balance of all images.

Distortion correction generates standard corner point coordinates through a standard checkerboard grid for camera calibration, and obtains camera internal parameters and mapping matrices, thereby completing the image calibration process. During the image capture process, the camera is stationary at a fixed position, so only one corner point detection is required.

There are many irrelevant noise points in the pre-processed image, which can be eliminated by pixel clustering and other methods, but at the same time, some plant pixels are distributed further on. This paper does not over-process the two-dimensional image in this part, but further improves it in the subsequent three-dimensional point cloud.

3.2. Three-Dimensional Plant Reconstruction Based on SFM-MVS

The three-dimensional morphological structure of plants can reflect the true state of plant growth and development. Establishing three-dimensional models of plants to study plants and accurately measure the height, volume, leaf inclination, and other parameters of plants have always been a research hotspot in botany, computer graphics, and other disciplines [25]. In this paper, we used the built-in functions of the commercial software Agisoft photoscan 1.3.2 (Agisoft LLC, ST, Petersburg, Russia) to detect feature points, generate sparse point clouds, and reconstruct dense point clouds in the above pre-processed image sequences. During the processing process, the software can automatically estimate camera movement trajectories and image coordinates. All data is generated on a computer with Windows 10 Professional system, CPU-Intel 12490F, graphics card NVIDIA GeForce 2060RTX, and 16G running memory. As shown in Figure 3 below, after loading the image sequence (a) processed in Figure 2 above, the adjacent image feature points are calculated to generate a plant sparse point cloud model (b) after depth image enhancement, point cloud calculation and registration, a dense point cloud model is formed (c) the time required for a single plant to build a dense point cloud is roughly distributed between 100–150 s. The number of original point clouds for a single plant is about 1.5–1.8 million. The point cloud data is finally exported and saved as a sphere of size 1.

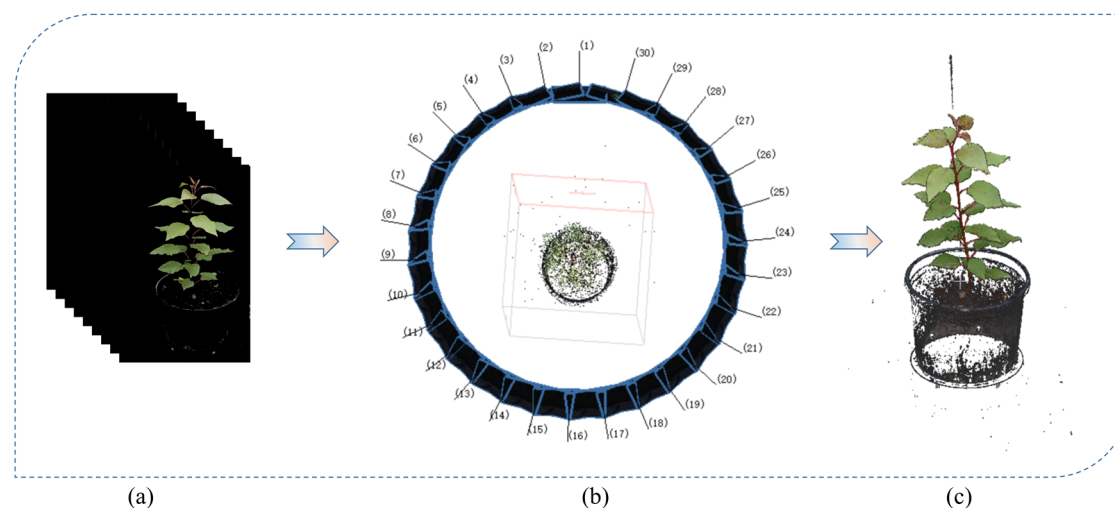


Figure 3. Plant point cloud reconstruction based on SFM-MVS. Illustration: (a) Image sequence after noise reduction; (b) Sparse point cloud reconstruction; (c) Dense point cloud reconstruction.

3.3. Point Cloud Noise Reduction and Calibration Processing

Due to the influence of multiple factors, such as the data acquisition method and the imaging background, the generated the point cloud information has a lot of outliers

and noise, including some point cloud information of pots, which is not conducive to the subsequent segmentation of plant organ instances, or will lead to the low accuracy of final phenotypic parameters. Point cloud noise reduction is required before three-dimensional feature analysis. Figure 4 shows the noise-reduction steps for point cloud data of a single poplar tree. As shown in (a) the first step is: a three-dimensional plant coordinate system is established with the gravity direction as the Z axis, and the XOY plane is represented as the ground. A spatial filter of the same size is set up to remove the point cloud outliers outside the distant region. The second step shown in (b) is based on the pot, the imaging background color threshold is very different from the plant itself, based on the overall point cloud RGB color threshold to eliminate pot and most of the background noise point clouds. The third step shown in (c) is to remove the abnormal point cloud value that cannot meet the clustering conditions based on the radius filtering function, that is, setting a radius search range and the minimum number of point clouds. If the condition that the number of point clouds in the search range of the range is greater than is not met, it will be regarded as an abnormal value removal. All noise reduction function parameter settings are shown in Table 3 below.

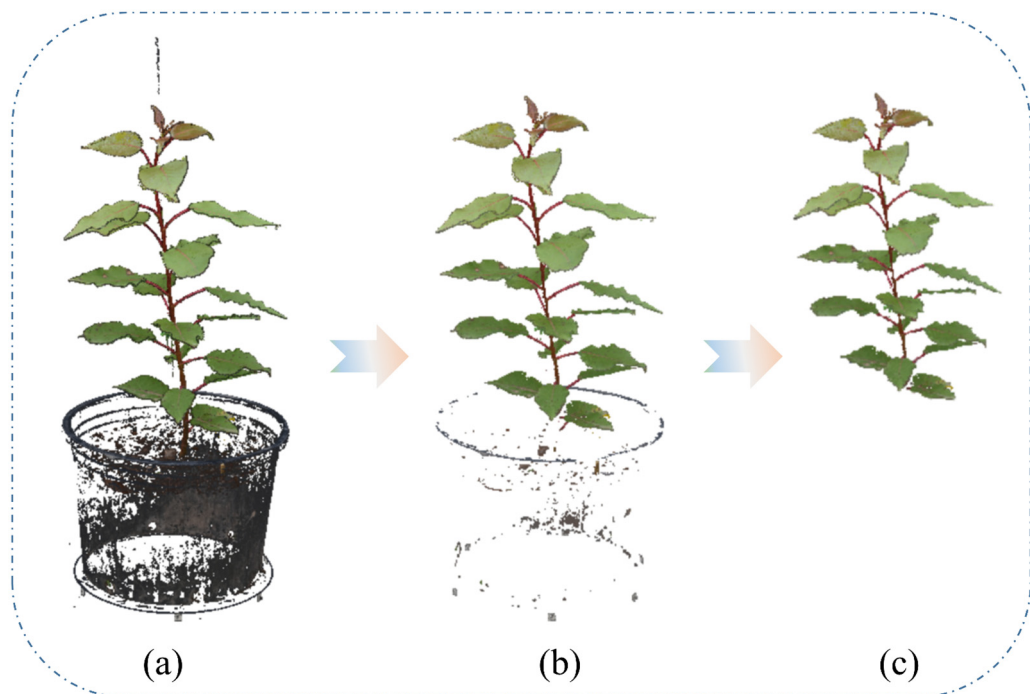


Figure 4. Point cloud noise reduction based on different filter functions. Illustration: (a) Spatial filtered point cloud; (b) Point cloud after color filtering; (c) Point cloud after radius filtering.

Table 3. Point cloud filter noise reduction function parameter setting.

Function Type	Parameter Setting		
Spatial filtering	X (m) 0.65	Y (m) 0.65	Z (m) 1.5
Color filtering	R 60	G 60	B 60
Radius filtering	r (mm) 0.5	n (a) 20	

Different from laser-type sensors, point clouds reconstructed by multi-view are affected by point cloud size, the camera position, angle, and configuration, and plant point clouds are often scaled inconsistently, which cannot reflect the true size of plants. In this study, point cloud information was used to describe the spatial distribution of chlorophyll

content on the whole plant. In order to directly reflect the relationship between chlorophyll distribution and plant morphology at different growth stages and under different water treatments, object point clouds with a known shape and size should be selected for calibration and calibration of plant point clouds. As shown in Figure 5, we selected the area where the pot is located, segmented the top, lower, and rotating disk plane of the pot based on the least square method of plane segmentation, and measured the radius $R1_{SFM}$, $R2_{SFM}$ and $R3_{SFM}$, respectively. The average ratio of the ratio with the actual measured radius value $R1$, $R2$ and $R3$ is used as the calibration scale of the plant point cloud, and the relationship is shown as follows.

$$\varphi = \frac{1}{3} \left(\frac{R1_{SFM}}{R1} + \frac{R2_{SFM}}{R2} + \frac{R3_{SFM}}{R3} \right) \quad (1)$$



Figure 5. Point cloud shape and size calibration.

After the noise reduction, the average number of poplar point clouds per tree is about 0.6 million, and the data storage capacity is 25–40 MB, which is suitable for subsequent processing, and no sampling processing is required.

4. Results and Analysis

The phenotypic variations in poplar plants are pronounced across distinct growth stages and under varied water treatments. Illustrated in Figure 6, average color information of the top and lower layers of the plants in the RGB color space was calculated by selecting regions of interest in the top frame of the two-dimensional image (Figure 6a–c). Model independent variables are selected by constructing the visible light vegetation index and conducting correlation analysis with chlorophyll (Figure 6d). Partial least squares regression (PLSR), support vector machine (SVM), and random forests (RF) are employed for inversion (Figure 6e). The regression value of the optimal model is then mapped to a fixed color gamut scale. By integrating this information with denoised three-dimensional point cloud color data, the three-dimensional distribution of poplar plant chlorophyll is achieved (f).

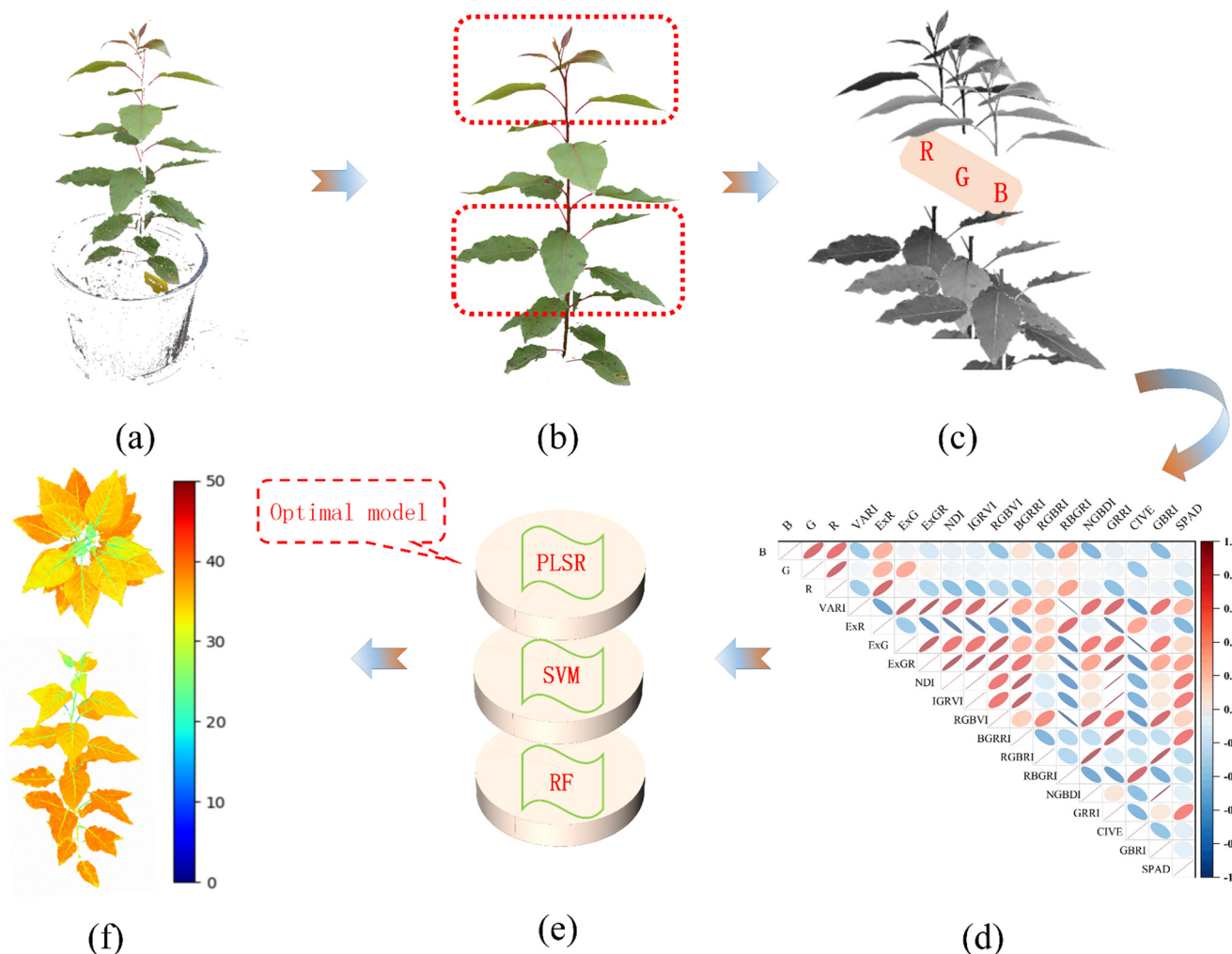


Figure 6. Processing flow of 3D distribution of poplar chlorophyll. Illustration: (a) Raw image; (b) Blade stratification; (c) Color feature extraction; (d) Variable selection; (e) model regression; (f) Visualization.

4.1. The Average Leaf Color Information Is Calculated Based on the Region of Interest

When calculating the color information of the top and lower leaves of poplar trees, all images of a single plant are traversed, and a custom function is used to select the area of interest in the mask image. Among them, the top part of the box numbered in the singular number is selected, other boxes select the lower part. In order to avoid the impact of the excessive redness of poplar leaf stems on the accuracy of the final data, we tried to keep only orthographic leaves selected during frame selection. The total value of single-channel pixels $P_i(P_j)$ and the number of pixels $n(m)$ in each layer's RGB color space was calculated after the top and lower frames were selected 15 times, respectively. After the area of interest is selected in the frame, in order to avoid the influence of background independent pixels on the final leaf color information calculation, the area of interest selected in the frame is further masked, and the calculation domain is only kept in the plant leaves itself. The average pixel values $\alpha(\beta)$ of R, G, and B of the top (or lower) leaves of a single poplar tree are obtained by comparing the total pixel value $P_i(P_j)$ of the above RGB single channel with the number of pixel points $n(m)$ of the top and lower leaves after mask. Finally, the values of the 15 images of the top and lower layers of a single poplar plant are averaged. The average RGB color information of the $\eta_{Top}(\eta_{Lower})$ blade is obtained, and the calculation principle is shown in Figure 7 below.

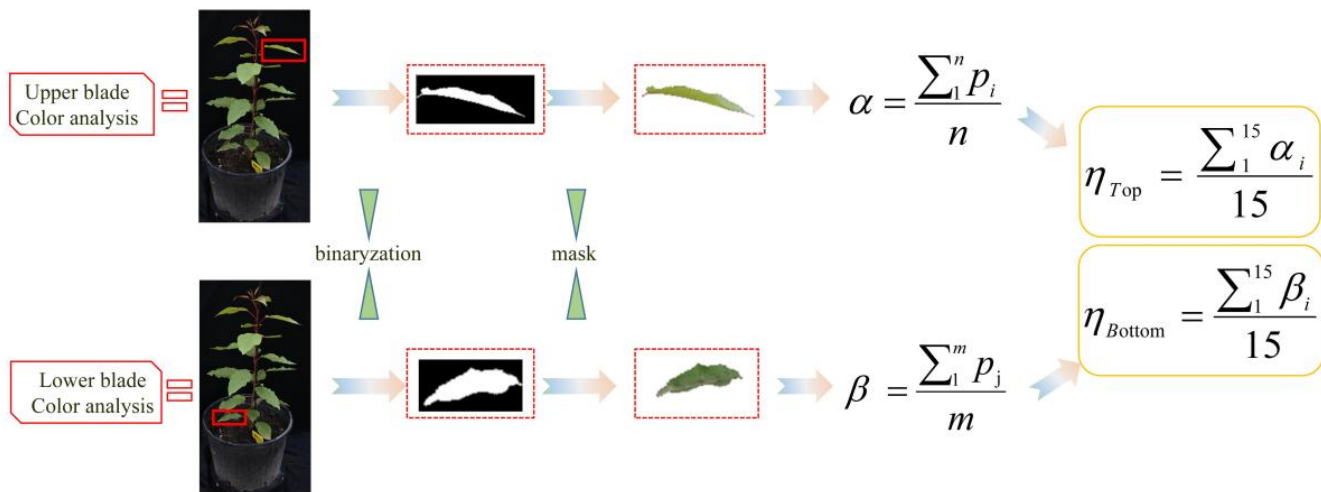


Figure 7. Calculation of color information of poplar stratified leaves. Illustration: P is the pixel value of R, G and B of a certain blade, n is the number of times the box of interest is selected; $\alpha(\beta)$ is the average pixel value of R, G, and B of the top (lower) leaves of a single poplar tree, $\eta_{Top}(\eta_{Lower})$ is the average pixel value of R, G, and B in the top (lower) layer of a single poplar tree.

4.2. Variable Feature Selection

The content and distribution of chlorophyll and other biochemical components in green plants will result in a large difference in the plant color [26–28]. After calculating the multi-color spatial information of leaves, this paper constructs a common vegetation index of 14 colors based on different function combinations of R, G, and B, including: normalized type color index, ratio type color index, composite color index, and three index types. This paper conducts the correlation analysis with the actual chlorophyll measurement. The specific calculation formula of RGB color index is shown in Table 4 below.

Table 4. Vegetation indices developed from RGB images.

Color Index Type	Color Index Name	Abbreviation	Formula
Normalized type color index	(visible-band difference vegetation index)	VDVI	$(2G - R - B) / (2G + R + B)$
	(normalized green-blue difference index)	NGBDI	$(G - B) / (G + B)$
	(visible atmospheric impedance vegetation index)	VARI	$(G - R) / (G + R - B)$
	(normalized difference index)	NDI	$(G - R) / (G + R)$
	(improved green-red vegetation index)	IGRVI	$(G - R^2) / (G + R^2)$
	(red-green-blue vegetation index)	RGBVI	$(G^2 - BR) / (G^2 + BR)$
Ratio type color index	(green-red ration index)	GRRI	G / R
	(blue-green red ration index)	BGRRI	$(G + B) / R$
	(red-green blue ration index)	RGBRI	$(G + R) / B$
	(red-blue green ration index)	RBGRI	$(R + B) / G$
Composite color index	(excess green index)	ExG	$2G - R - B$
	(excess red index)	ExR	$1.4R - G$
	(green-red difference vegetation index)	ExGR	$ExG - ExR$
	(color index of vegetation)	CIVE	$0.411R - 0.881 + 0.385 + 18.7578$

According to the results of correlation analysis, the higher correlation value ExR, normalized difference index NDI, improved green-red vegetation index IGRVI, blue-green

anti-red vegetation index BGRRI, and green-red ratio index GRRI were selected as the input variables of the model, and their correlation values were distributed in the range of 0.61–0.66.

In this study, a total of 480 poplar sample image data was obtained from five growth stages before and after drought, and the color information of each plant was calculated by dividing the top layer and the lower layer, respectively, that is, 960 sample data were obtained. Three common machine learning algorithms RF, SVM and PLSR, were selected to establish regression models. 2/3 ($n = 640$) were randomly selected for training each model, and 1/3 ($n = 320$) was used to experiment the accuracy of each model. The coefficient of determination (R^2) and root mean-square error (RMSE) was used to evaluate the accuracy and applicability of each model. Figure 8 shows the regression accuracy results of each model test set.

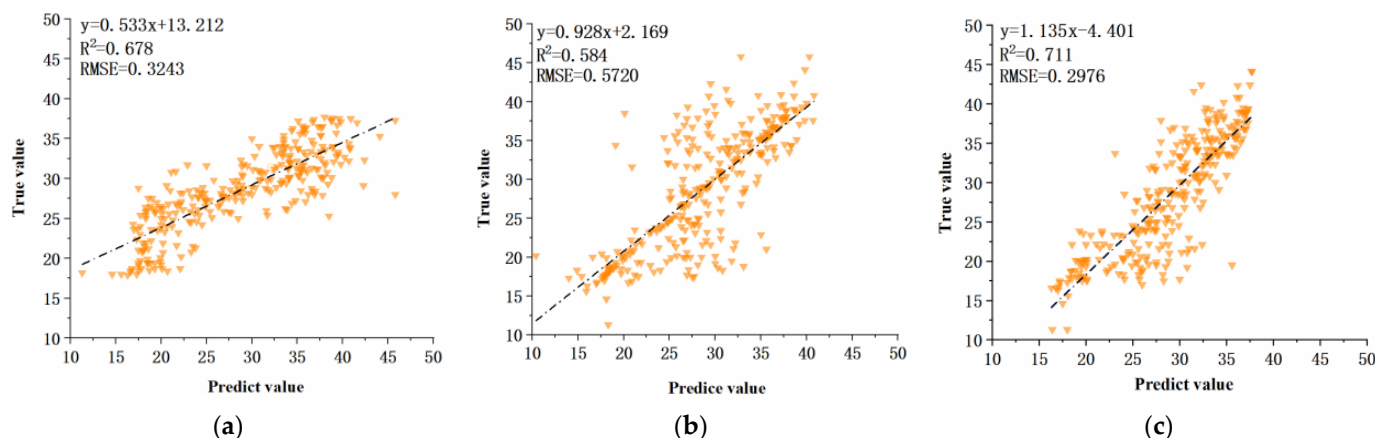


Figure 8. Regression results of each model. Illustration: (a) RF; (b) SVM; (c) PLSR.

In order to ensure the final unity of variables, all independent variable data were normalized before input into the model. According to the regression results of each model, PLSR experiment set has the highest regression accuracy, with R^2 of 0.711 and RMSE of 0.2976. Compared with other machine learning algorithms, PLSR is a regression algorithm that considers the contribution of principal components to dependent variables. The regression mode in this study is shown in Equation (2) below:

$$y = -0.2505 * ExR - 1.781 * NDI * 10^4 + 8.025 * IGRVI * 10^3 + 32.55 * BGRRI + 8.329 * GRRI * 10^2 - 849.9 \quad (2)$$

where y represents the predicted value of chlorophyll content.

4.3. Visualization of 3D Distribution of Poplar Chlorophyll

Using computer graphics and image processing technology to fuse multi-dimensional image data to intuitively reflect difficult-to-measure phenotypic data, plant growth can be evaluated with more comprehensive information [29]. Three-dimensional point clouds can effectively avoid the limitations of unclear and inaccurate phenotypic data caused by occlusion problems. The point cloud model contains not only the surface shape and texture information of plants, but also the color information of plants themselves, which provides rich independent variables for directly using mathematical models to change plant point clouds [30].

The point cloud information of poplar seedlings in multiple growth stages was obtained. The color information of the top and lower layers of two-dimensional plant images was combined with the PLSR model of chlorophyll actual measurement value inversion, and the point cloud color information was combined to realize visualization, which can be divided into the following steps. (1) read points cloud information; (2) traverse all point clouds and calculate the RGB color value of each point cloud; (3) define PLSR regression

model; (4) calculate and set the uniform color mapping maximum value; (5) render the point cloud by the computed value of the function, and convert it into the color algorithm commonly used in computer vision COLORMAP_JET; (6) output the rendered point cloud and print the gamut ruler.

In the process of visualization, the maximum value and minimum value of chlorophyll of different poplar plants is not uniform, and the final COLORMAP mapping to false color image is based on the unified mapping of the minimum value to the maximum value of plants. In order to avoid the color mapping of the same chlorophyll content value in different plant point clouds is inconsistent, resulting in the failure to form effective numerical comparison of chlorophyll content in different plant point clouds. It is necessary to calculate the maximum and minimum values obtained by the cloud files in the model in advance, and redefine a mapping color maximum interval to make the range larger than the maximum value interval calculated by the model, so as to ensure that the same chlorophyll content is mapped to the same color under different varieties, different growth periods and different water treatments.

We selected representative plants in this experiment for the following visualization. Figure 9a shows the three-dimensional distribution of chlorophyll of the same poplar tree from the first to the fourth week; Figure 9b shows different drought levels. Response to changes in chlorophyll of 110 *poplar* under normal growth; Figure 9c shows from left to right the changes in chlorophyll distribution of four poplar varieties, 3804 *poplar*, 110 *poplar*, SY-1 *poplar* and 895 *poplar*, before and after being cultivated with the same drought intensity for 15 days; at the same time, in order to intuitively quantify the changes in chlorophyll content of poplar trees at various stages in this study, Figure 10 we calculated the total average chlorophyll content of the upper and lower leaves of the four poplar varieties at different periods, and used the quantitative analysis of Figure 10 combined with the three-dimensional visualization diagrams of Figure 9a–c, the following overall overview of this experimental study is made.

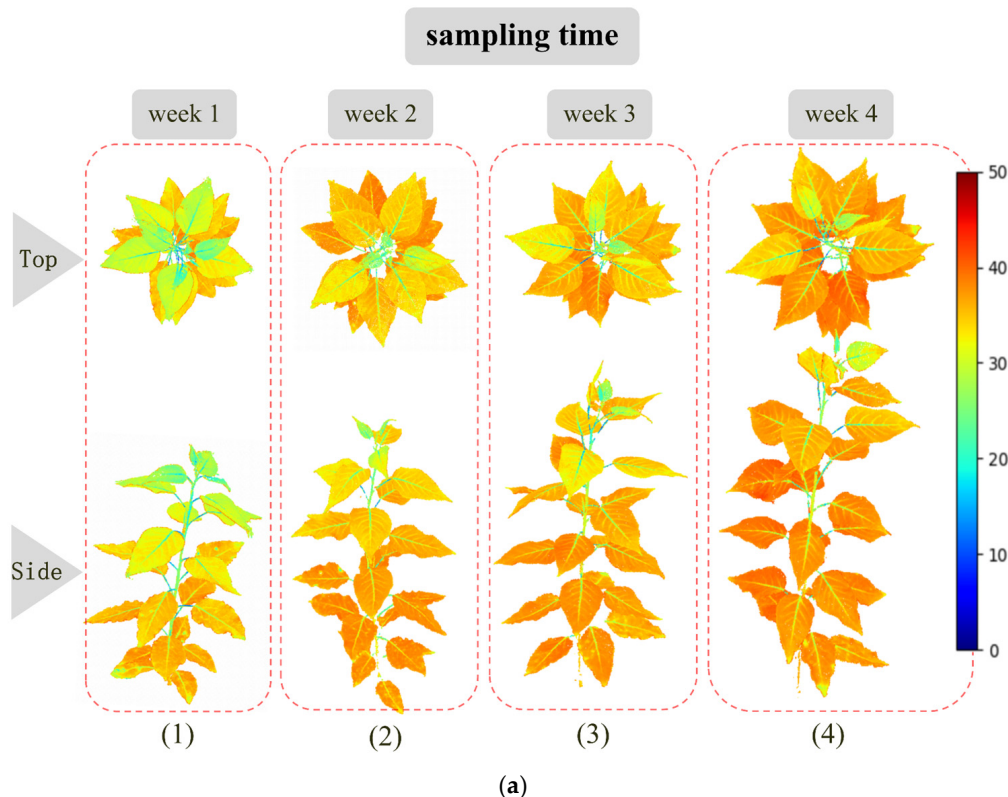


Figure 9. Cont.

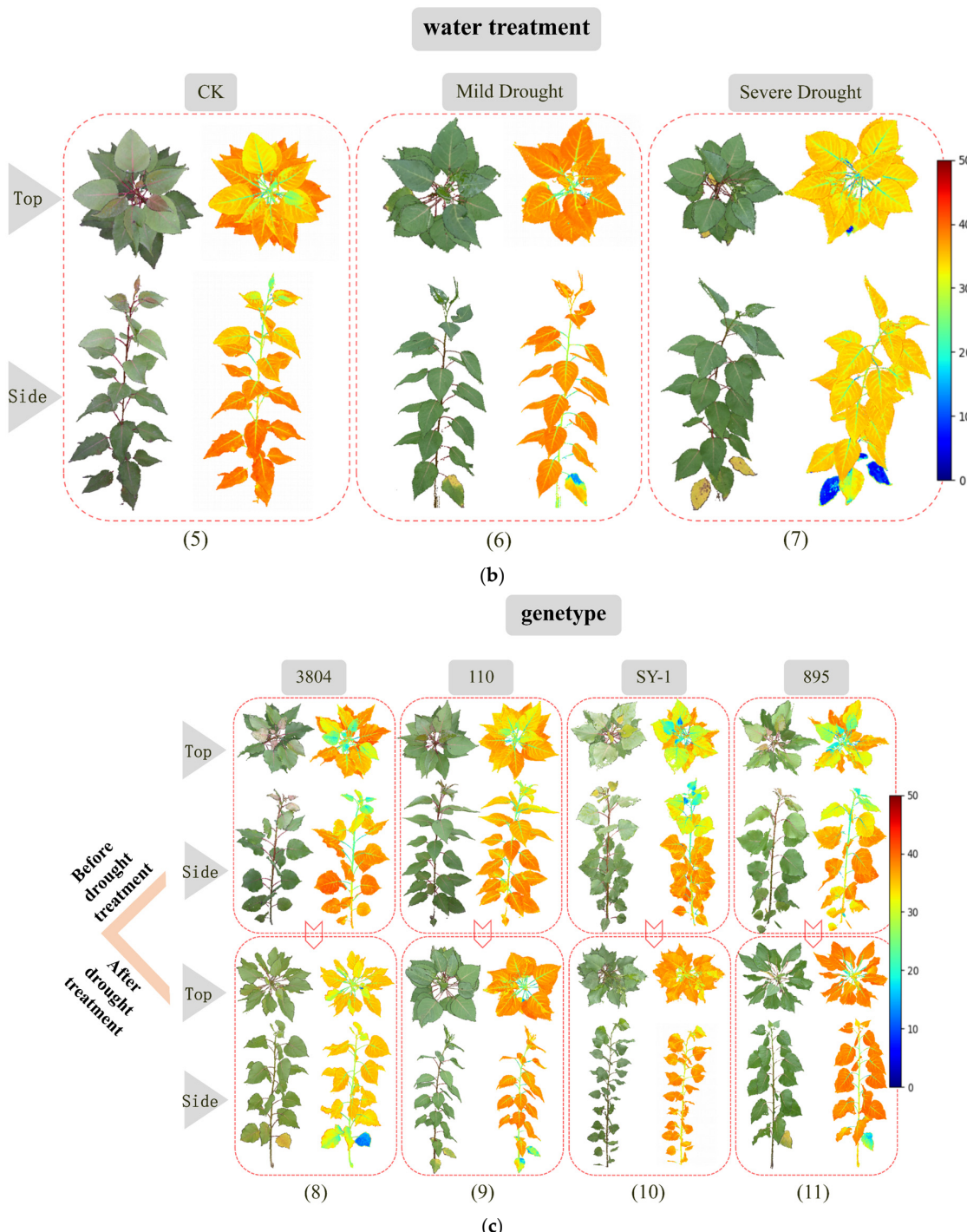


Figure 9. Chlorophyll three-dimensional visualization at each stage of the test. (a) 3D visualization of poplar chlorophyll at different growth stages (Illustration: Pictures (1), (2), (3), and (4), respectively, correspond to the three-dimensional chlorophyll visualization model of the same plant from week 1 to week 4). (b) 3D visualization of 110poplar chlorophyll under different water treatments (Illustration: Pictures (5), (6), and (7), respectively, correspond to the three-dimensional chlorophyll visualization model of the same genotype (110) under different drought treatment levels). (c) Three-dimensional visualization of chlorophyll under different gene regulation (Illustration: Pictures (8), (9), (10), and (11), respectively, correspond to the three-dimensional chlorophyll visualization points of the four poplar varieties 3804, 110, SY-1, and 895 from before drought treatment (upper dotted line box) to after drought treatment (lower dotted line box) cloud model).

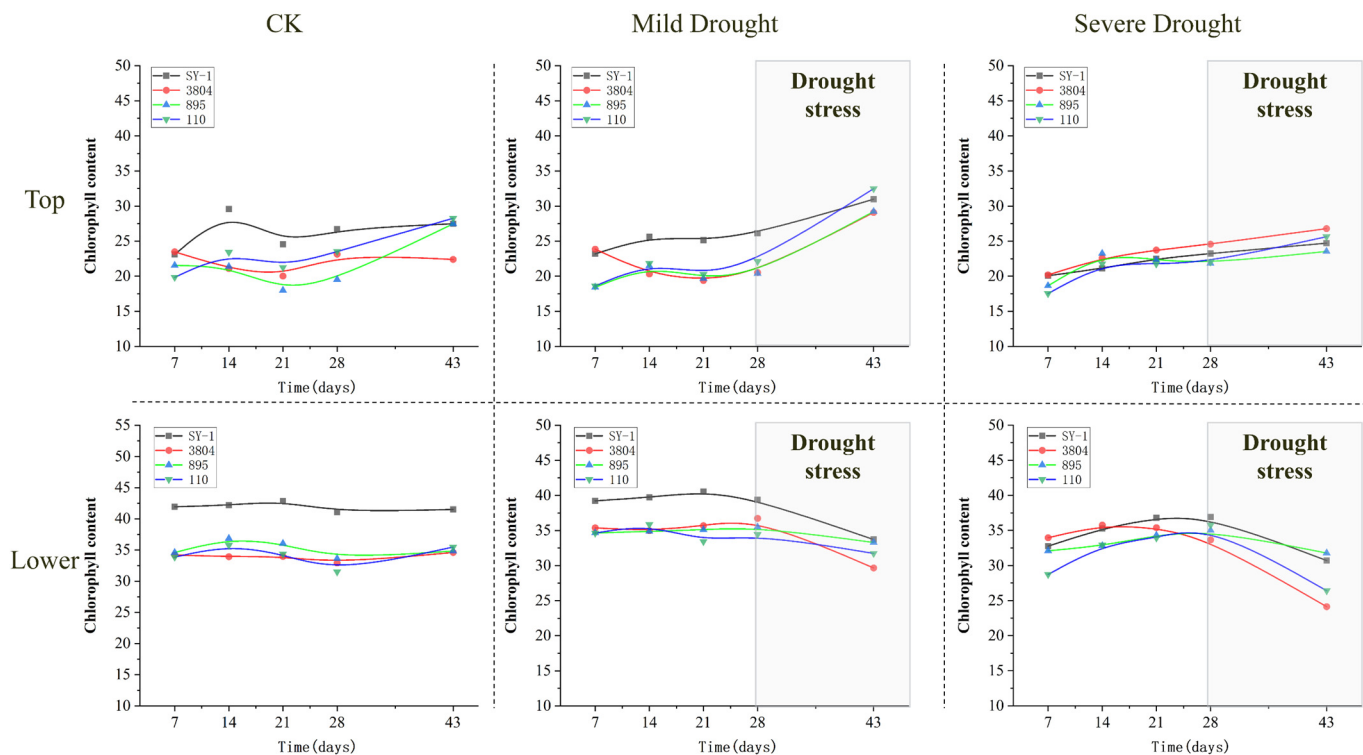


Figure 10. Chlorophyll content response at each stage of the test. Illustration: CK, mild drought, and severe drought in the figure represent the three levels of drought culture, respectively; top and lower represents upper leaves and lower leaves, and the time when drought begins is the 28th to 43rd day after the start of the experiment.

The first to fourth sub-pictures in Figure 9a are the chlorophyll three-dimensional visualization models from the first to the fourth week when data collection begins. Under natural growth conditions, the chlorophyll content of poplar saplings gradually accumulates with the time of photosynthesis. The newly grown leaves in the upper layer have a short photosynthesis time and a relatively low chlorophyll content; the lower leaves have a long growth time. Photosynthesis takes a relatively long time, and the accumulation of chlorophyll results in higher values. The chlorophyll is roughly distributed vertically between individual poplar trees. The chlorophyll content of the lower leaves is higher than that of the upper leaves. This is also consistent with the analysis results of each culture group before the 28th day of the experiment in Figure 10.

Figure 9b shows the original point cloud and the visualized point cloud of 110 poplar under different drought levels. The control checks (CK) group model shown in picture (5), sufficient water conditions provide plants with energy for photosynthesis. The plant maintains normal growth status, and chlorophyll is still distributed gradually from top to bottom among the poplar trees; in the severe drought group shown in picture (7), severe water shortage in the plants caused the leaves to wilt and turn yellow, increase the inclination angle in a short period of time, limit photosynthesis, some leaves have fallen off, and the overall chlorophyll content dropped sharply. But at the same time, from picture (6) combined with the analysis results in Figure 10, the consistent point between severe drought and mild drought is that the upper leaves of the four varieties of poplar trees still have slightly increased values, and the elevated value in the mild drought group was greater than that in the severe drought group.

Figure 9c shows the changes in the three-dimensional chlorophyll distribution of four poplar varieties within 15 days before and after mild drought stress. From the visual model shown in pictures (8), (9), (10), (11), before the onset of drought stress (upper dotted line box), the poplar trees of the four genotypes all showed a longitudinal gradient distribution of chlorophyll. The difference in chlorophyll distribution between different varieties was not

obvious, but significant changes occurred after drought stress (lower dotted line box), at this time, the average chlorophyll content of the four varieties was $895 > SY-1 > 110 > 3804$. At the same time, the chlorophyll change rate of the four poplar genotypes before and after drought showed great differences. The change rate of chlorophyll content of the upper leaves was $110 > 895 > 3804 > SY-1$, and the change rate of chlorophyll content of the lower leaves was $3804 > SY-1 > 110 > 895$.

It can be seen that factors such as different degrees of drought and inconsistent drought resistance of plants will lead to large differences in the chlorophyll content of poplar seedlings under the same cultivation conditions. Drought stress can trigger physiological responses such as plant stomatal closure, leaf degradation, oxidative damage, and photosynthesis inhibition. Moderate drought severity and drought duration will actually increase the chlorophyll content of plants. This conclusion has also been explained in a large number of research [30]. The three-dimensional digital identification of chlorophyll through point cloud information not only greatly enhances the intuitiveness of the human eye in detecting changes in chlorophyll content, but also by observing the distribution of chlorophyll among the organs of poplar trees, we can analyze the response mechanism of chlorophyll content in different organs such as leaves and stems of plants under drought stress, so as to efficiently characterize the degree of plant stress and quickly take solutions. The research provides technical support and decision-making support for early diagnosis of poplar drought conditions, adjusting the ecological adaptability of varieties, and optimizing cultivation and management techniques.

5. Discussion

SFM-MVS technology is a three-dimensional reconstruction technology that can automatically estimate camera arrays based on image sequences. In this study, it provides us with an imaging form in which the camera is stationary and the plant is rotating, achieving image sequence illumination in a short period of time unification, which establishes prerequisites for subsequent unified image color correction and subject segmentation [31]. In addition, the density and quality of point clouds presented by integrated three-dimensional imaging sensors, such as LIDAR and RGB-D cameras, are limited and cannot well display the color information of the leaf surface, let alone provide visible light image data sets for building models. In contrast, SFM-MVS technology has become a low-cost, lightweight three-dimensional phenotyping research method [32]. At the same time, as a result of technical advances, such as the Lumalabs model, more methods of computer vision and image processing have been reported. Therefore, it is reasonable to anticipate that a method detecting plant phenotyping could be developed to provide chlorophyll content more intelligently.

Although the validation results demonstrated the potential of the new technology, a few limitations are noted and should be worked on to improve the method. First, when we identify stress conditions, other non-invasive methods, such as chlorophyll fluorescence analysis, yield better results in the early stages of analysis. The cost is high and it also requires high imaging environment, so most of the research scale focuses on leaf or smaller plant. However, in this study, the plant height could reach 1.2–1.5 m in the later stages of the experiment. Using chlorophyll fluorescence equipment to non-invasively achieve three-dimensional parameter measurement and phenotype visualization of the entire plant will be challenging, but we still need to try it out in practice. Secondly, this study tested the 3D quantification and visualization performance of chlorophyll content in poplar seedling leaves, which is a key step in demonstrating the use of SFM-MVS technology combined with machine learning to link the three-dimensional distribution changes of chlorophyll in poplar under drought stress. The poplar saplings used to test the new method have a relatively simple plant structure and small leaves, compared to mature poplar. The denser leaf structure of this growth stage makes it more challenging to capture the complete point cloud of the canopy (due to occlusion), and more and larger leaves further reduce the efficiency for surface reconstruction.

In this study, we found that the chlorophyll content of the upper leaves of poplar trees of the same species accumulated after experiencing drought stress. Low-intensity and short-term drought stress causes plant leaves to retain water and self-regulate, and the stomata of the leaves are closed to limit the entry of carbon dioxide. In order to adapt to their own photosynthesis, plants will increase the content of chlorophyll to improve light energy absorption and utilization efficiency. To balance the adverse effects of stomatal closure to limit carbon dioxide absorption, the chlorophyll content of the upper leaves increased compared with normal culture. This result is consistent with the conclusions in the literature [33,34].

Different drought stress levels can cause different fluctuations in plant physiological and metabolic activities. Plants cultured under different drought conditions response mechanisms of chlorophyll content in different poplar varieties may or may not be the same [35,36]. The use of computer technology to identify the three-dimensional distribution of chlorophyll content is of great significance for the early detection of plant drought stress. For forestry production, early detection and characterization of crop drought conditions can help forestry producers take a series of measures such as increasing irrigation, improving soil moisture management, and shading as early as possible to reduce production losses in forestry production and improve yield quality. For scientific research, efficient characterization of plant water loss can help scholars better understand the physiology and response mechanisms of plants under drought stress, adjust the applicability of different germplasm in different ecosystems, and promote research and development of technological strategies to combat drought, cultivate excellent drought-resistant varieties, and protect the diversity of ecosystems [37].

However, in the context of the inability to fuse multi-band reflectivity and three-dimensional structural information of plants through a single sensor, achieving organ-level high-precision three-dimensional digital identification of plant physical and chemical phenotypic parameters faces huge challenges, as shown in the literature [38–41], scholars use existing optical sensors to obtain point cloud information of soybeans, lettuce and small potted plants to achieve plant morphological phenotype information assessment such as segmentation and counting of organs between plants. However, physical and chemical parameters such as chlorophyll, nitrogen content, and water content are difficult to detect. The study of vertical distribution in three-dimensional plant models still lacks extensive research and development. At the same time, due to the lack of a mature point cloud annotation environment and the huge amount of calculations, it is impossible to build an efficient deep learning model to achieve efficient segmentation and phenotypic identification of rich data sets in a short time, which greatly restricted the multi-dimensional and high-level intelligent development of plant phenomics [42].

In the future, improvements in data acquisition and measurement methods should be considered, and spectral analysis technology should be considered in three-dimensional models to improve the final data dimension and phenotypic identification accuracy. The three-dimensional modeling technology based on the SFM-MVS technology can restore the details of the plant itself with high accuracy, however, compared with large-scale, high-throughput rapid identification of plant phenotypes, it is more suitable for supporting greenhouse seedling cultivation. High-accuracy plant point cloud information can be integrated with computer science technology to provide effective technology for obtaining seedling phenotypes, as a means to promote the cultivation of fine varieties and analyze the phenotypic parameter responses of various plant organs under stress conditions.

6. Conclusions

This paper proposes a three-dimensional plant chlorophyll visualization technology based on a machine learning model that renders point cloud colors. The experimental results of three-dimensional point cloud models of four varieties of poplar before and after water stress show. Image pre-processing can effectively reduce the amount of image storage and improve the accuracy and speed of point cloud reconstruction. The model

that uses plant correction multi-view image information to invert chlorophyll content has high accuracy, among which the R^2 of the PLSR model is 0.711. This model is integrated with plant point cloud correction color values to realize the chlorophyll content of poplar saplings under the condition of rich sample data sets. Three-dimensional identification is used to comparatively analyze the chlorophyll content response of multiple poplar varieties under different growth periods, different gene regulation, and different drought levels.

Based on the method proposed in this article, sensing the vertical spatial distribution of plant chlorophyll among plants has become a low-cost, efficient, and intuitive method, which can be used to better identify plant trait changes in the early stages of stress and make improvement decisions in advance. This study found that under normal cultivation, the chlorophyll content of four poplar varieties showed a vertical gradient distribution state gradually increasing from top to bottom among the plants; under low-intensity, short-term drought stress, the upper leaves of poplar saplings that chlorophyll content showed a cumulative phenomenon and the value increased, if the drought intensity is low, the stronger the cumulative effect. In the lower leaves, the chlorophyll value decreased significantly with insufficient water supply. The value decreased in the severe drought group is greater than that in the mild drought group.

Although the chlorophyll content of the upper leaves increased and the chlorophyll content of the lower leaves decreased in the four poplar genotypes after drought stress, the numerical changes were quite different. The differences among varieties are not only reflected in the light interception ability and light energy utilization efficiency of the leaves, but also in the inconsistent water absorption capacity between organs. These are the main factors affecting chlorophyll synthesis. As a result, the change rate of chlorophyll content of drought-tolerant varieties SY-1 and 3804 before and after drought stress was lower than that of poplars 895 and 110. Utilizing the chlorophyll response mechanisms of different varieties under drought stress can provide an effective reference for regulating and planting suitable tree species in different ecological regions.

Author Contributions: Q.T.: writing—original draft, software, methodology. H.Z.: writing—review and editing, funding acquisition, project administration. L.B.: supervision, conceptualization. L.Z. and Y.G.: writing—review and editing. All authors have read and agreed to the published version of the manuscript.

Funding: This work is supported by National Key Research and Development Program of China (2023YFE0123600), National Natural Science Foundation of China (NSFC 32171790, 32171818, and 62305166) and Jiangsu Province agricultural science and technology independent innovation fund project (CX(23)3126).

Data Availability Statement: The data are not publicly available because this study is still in progress.

Acknowledgments: The authors would like to thank Lu Wang and Ziyang Zhou, for their help and advice in the study.

Conflicts of Interest: The authors declare that they have no known competing financial interest or personal relationship that could have appeared to influence the work reported in this paper.

References

1. Wilhite, D.A. (Ed.) *Drought Assessment, Management, and Planning: Theory and Case Studies*; Springer: Boston, MA, USA, 1993; ISBN 978-1-4613-6416-0.
2. Rosso, L.; Cantamessa, S.; Bergante, S.; Biselli, C.; Fricano, A.; Chiarabaglio, P.M.; Gennaro, M.; Nervo, G.; Secchi, F.; Carra, A. Responses to Drought Stress in Poplar: What Do We Know and What Can We Learn? *Life* **2023**, *13*, 533. [[CrossRef](#)] [[PubMed](#)]
3. Seleiman, M.F.; Al-Suhaiibani, N.; Ali, N.; Akmal, M.; Alotaibi, M.; Refay, Y.; Dindaroglu, T.; Abdul-Wajid, H.H.; Battaglia, M.L. Drought Stress Impacts on Plants and Different Approaches to Alleviate Its Adverse Effects. *Plants* **2021**, *10*, 259. [[CrossRef](#)] [[PubMed](#)]
4. Porcar-Castell, A.; Malenovský, Z.; Magney, T.; Van Wittenberghe, S.; Fernández-Marín, B.; Maignan, F.; Zhang, Y.; Maseyk, K.; Atherton, J.; Albert, L.P.; et al. Chlorophyll a Fluorescence Illuminates a Path Connecting Plant Molecular Biology to Earth-System Science. *Nat. Plants* **2021**, *7*, 998–1009. [[CrossRef](#)] [[PubMed](#)]

5. Feng, H.; Chen, G.; Xiong, L.; Liu, Q.; Yang, W. Accurate Digitization of the Chlorophyll Distribution of Individual Rice Leaves Using Hyperspectral Imaging and an Integrated Image Analysis Pipeline. *Front. Plant Sci.* **2017**, *8*, 1238. [[CrossRef](#)] [[PubMed](#)]
6. Becker, E.; Schmidhalter, U. Evaluation of Yield and Drought Using Active and Passive Spectral Sensing Systems at the Reproductive Stage in Wheat. *Front. Plant Sci.* **2017**, *8*, 379. [[CrossRef](#)] [[PubMed](#)]
7. Zhang, Y.; He, N.; Yu, G. Opposing Shifts in Distributions of Chlorophyll Concentration and Composition in Grassland under Warming. *Sci. Rep.* **2021**, *11*, 15736. [[CrossRef](#)] [[PubMed](#)]
8. Amutenya, A.; Kwembeya, E.; Shikangalah, R.; Tsvuura, Z. Photosynthesis, Chlorophyll Content and Water Potential of a Mistletoe-Host Pair in a Semi-Arid Savanna. *S. Afr. J. Bot.* **2023**, *163*, 311–315. [[CrossRef](#)]
9. Karami, E.; Weaver, J.B. Dry-Matter Production, Yield, Photosynthesis, Chlorophyll Content and Specific Leaf Weight of Cotton in Relation to Leaf Shape and Colour. *J. Agric. Sci.* **1980**, *94*, 281–286. [[CrossRef](#)]
10. Zhang, H.; Ge, Y.; Xie, X.; Atefi, A.; Wijewardane, N.K.; Thapa, S. High Throughput Analysis of Leaf Chlorophyll Content in Sorghum Using RGB, Hyperspectral, and Fluorescence Imaging and Sensor Fusion. *Plant Methods* **2022**, *18*, 60. [[CrossRef](#)]
11. Liu, W.; Li, Y.; Tomasetto, F.; Yan, W.; Tan, Z.; Liu, J.; Jiang, J. Non-Destructive Measurements of *Toona Sinensis* Chlorophyll and Nitrogen Content Under Drought Stress Using Near Infrared Spectroscopy. *Front. Plant Sci.* **2022**, *12*, 809828. [[CrossRef](#)]
12. Li, Q.; Yan, Y.; Li, W. Coarse-to-Fine Segmentation of Individual Street Trees from Side-View Point Clouds. *Urban For. Urban Green.* **2023**, *89*, 128097. [[CrossRef](#)]
13. Jiang, H.; Zhou, Y.; Zhang, C.; Yuan, W.; Zhou, H. Evaluation of Dual-Band Near-Infrared Spectroscopy and Chemometric Analysis for Rapid Quantification of Multi-Quality Parameters of Soy Sauce Stewed Meat. *Foods* **2023**, *12*, 2882. [[CrossRef](#)] [[PubMed](#)]
14. Li, Q.; Xue, Y. Real-Time Detection of Street Tree Crowns Using Mobile Laser Scanning Based on Pointwise Classification. *Biosyst. Eng.* **2023**, *231*, 20–35. [[CrossRef](#)]
15. Wu, S.; Wen, W.; Wang, Y.; Fan, J.; Wang, C.; Gou, W.; Guo, X. MVS-Pheno: A Portable and Low-Cost Phenotyping Platform for Maize Shoots Using Multiview Stereo 3D Reconstruction. *Plant Phenomics* **2020**, *2020*, 1848437. [[CrossRef](#)] [[PubMed](#)]
16. Wang, Y.; Chen, Y. Non-Destructive Measurement of Three-Dimensional Plants Based on Point Cloud. *Plants* **2020**, *9*, 571. [[CrossRef](#)] [[PubMed](#)]
17. Hosoi, F.; Umeyama, S.; Kuo, K. Estimating 3D Chlorophyll Content Distribution of Trees Using an Image Fusion Method Between 2D Camera and 3D Portable Scanning Lidar. *Remote Sens.* **2019**, *11*, 2134. [[CrossRef](#)]
18. Bayati, H.; Najafi, A.; Vahidi, J.; Gholamali Jalali, S. 3D Reconstruction of Uneven-Aged Forest in Single Tree Scale Using Digital Camera and SfM-MVS Technique. *Scand. J. For. Res.* **2021**, *36*, 210–220. [[CrossRef](#)]
19. Westoby, M.J.; Brasington, J.; Glasser, N.F.; Hambrey, M.J.; Reynolds, J.M. ‘Structure-from-Motion’ Photogrammetry: A Low-Cost, Effective Tool for Geoscience Applications. *Geomorphology* **2012**, *179*, 300–314. [[CrossRef](#)]
20. Yao, Y.; Shu, S.; Wang, W.; Liu, R.; Wang, Y.; Wang, X.; Zhang, S. Growth and Carbon Sequestration of Poplar Plantations on the Tibetan Plateau. *Ecol. Indic.* **2023**, *147*, 109930. [[CrossRef](#)]
21. Semerci, A.; Guevara, C.A.; Gonzalez-Benecke, C.A. Water Availability Effects on Growth and Phenology of 11 Poplar Cultivars Growing in Semiarid Areas in Turkey. *New For.* **2021**, *52*, 411–430. [[CrossRef](#)]
22. Hassanjalilian, O.; Igathinathane, C.; Doetkott, C.; Bajwa, S.; Nowatzki, J.; Haji Esmaeili, S.A. Chlorophyll Estimation in Soybean Leaves Infield with Smartphone Digital Imaging and Machine Learning. *Comput. Electron. Agric.* **2020**, *174*, 105433. [[CrossRef](#)]
23. Ngugi, L.C.; Abelwahab, M.; Abo-Zahhad, M. Recent Advances in Image Processing Techniques for Automated Leaf Pest and Disease Recognition—A Review. *Inf. Process. Agric.* **2021**, *8*, 27–51. [[CrossRef](#)]
24. Li, Y.; Xia, H.; Liu, Y.; Ji, K.; Huo, L.; Ni, C. Research on Morphological Indicator Extraction Method of *Pinus Massoniana* Lamb. Based on 3D Reconstruction. *Forests* **2023**, *14*, 1726.
25. Huo, L.; Liu, Y.; Yang, Y.; Zhuang, Z.; Sun, M. Review: Research on Product Surface Quality Inspection Technology Based on 3D Point Cloud. *Adv. Mech. Eng.* **2023**, *15*, 16878132231159523. [[CrossRef](#)]
26. Teshome, D.T.; Zharare, G.E.; Naidoo, S. The Threat of the Combined Effect of Biotic and Abiotic Stress Factors in Forestry Under a Changing Climate. *Front. Plant Sci.* **2020**, *11*, 601009. [[CrossRef](#)] [[PubMed](#)]
27. Yuan, Y.; Wang, X.; Shi, M.; Wang, P. Performance Comparison of RGB and Multispectral Vegetation Indices Based on Machine Learning for Estimating *Hopea Hainanensis* SPAD Values under Different Shade Conditions. *Front. Plant Sci.* **2022**, *13*, 928953. [[CrossRef](#)] [[PubMed](#)]
28. Barrero, O.; Perdomo, S.A. RGB and Multispectral UAV Image Fusion for Gramineae Weed Detection in Rice Fields. *Precis. Agric.* **2018**, *19*, 809–822. [[CrossRef](#)]
29. Peng, C.; Li, S.; Miao, Y.; Zhang, Z.; Zhang, M. Stem-leaf segmentation and phenotypic trait extraction of tomatoes using three-dimensional point cloud. *Trans. Chin. Soc. Agric. Eng.* **2022**, *38*, 187–194.
30. Zermas, D.; Morellas, V.; Mulla, D.; Papanikolopoulos, N. 3D Model Processing for High Throughput Phenotype Extraction—The Case of Corn. *Comput. Electron. Agric.* **2020**, *172*, 105047. [[CrossRef](#)]
31. Fariaszevska, A.; Aper, J.; Van Huylenbroeck, J.; De Swaef, T.; Baert, J.; Pecio, Ł. Physiological and Biochemical Responses of Forage Grass Varieties to Mild Drought Stress Under Field Conditions. *Int. J. Plant Prod.* **2020**, *14*, 335–353. [[CrossRef](#)]
32. Iglhaut, J.; Cabo, C.; Puliti, S.; Piermattei, L.; O'Connor, J.; Rosette, J. Structure from Motion Photogrammetry in Forestry: A Review. *Curr. For. Rep.* **2019**, *5*, 155–168. [[CrossRef](#)]

33. Zhang, J.; Lin, X. Advances in Fusion of Optical Imagery and LiDAR Point Cloud Applied to Photogrammetry and Remote Sensing. *Int. J. Image Data Fusion* **2017**, *8*, 1–31. [[CrossRef](#)]
34. Rustioni, L.; Bianchi, D. Drought Increases Chlorophyll Content in Stems of Vitis Interspecific Hybrids. *Theor. Exp. Plant Physiol.* **2021**, *33*, 69–78. [[CrossRef](#)]
35. Sakya, A.T.; Sulistyaningsih, E.; Indradewa, D.; Purwanto, B.H. Stomata Character and Chlorophyll Content of Tomato in Response to Zn Application under Drought Condition. *IOP Conf. Ser. Earth Environ. Sci.* **2018**, *142*, 012033. [[CrossRef](#)]
36. Gai, J.; Wang, J.; Xie, S.; Xiang, L.; Wang, Z. Spectroscopic Determination of Chlorophyll Content in Sugarcane Leaves for Drought Stress Detection. *Precis. Agric.* **2023**. [[CrossRef](#)]
37. Yudina, P.K.; Ivanova, L.A.; Ronzhina, D.A.; Zolotareva, N.V.; Ivanov, L.A. Variation of Leaf Traits and Pigment Content in Three Species of Steppe Plants Depending on the Climate Aridity. *Russ. J. Plant Physiol.* **2017**, *64*, 410–422. [[CrossRef](#)]
38. Li, Z.; Guo, R.; Li, M.; Chen, Y.; Li, G. A Review of Computer Vision Technologies for Plant Phenotyping. *Comput. Electron. Agric.* **2020**, *176*, 105672. [[CrossRef](#)]
39. Li, D.; Shi, G.; Kong, W.; Wang, S.; Chen, Y. A Leaf Segmentation and Phenotypic Feature Extraction Framework for Multiview Stereo Plant Point Clouds. *IEEE J. Sel. Top. Appl. Earth Obs. Remote Sens.* **2020**, *13*, 2321–2336. [[CrossRef](#)]
40. Ma, X.; Wei, B.; Guan, H.; Yu, S. A Method of Calculating Phenotypic Traits for Soybean Canopies Based on Three-Dimensional Point Cloud. *Ecol. Inform.* **2022**, *68*, 101524. [[CrossRef](#)]
41. Zhang, Y.; Li, M.; Li, G.; Li, J.; Zheng, L.; Zhang, M.; Wang, M. Multi-Phenotypic Parameters Extraction and Biomass Estimation for Lettuce Based on Point Clouds. *Measurement* **2022**, *204*, 112094. [[CrossRef](#)]
42. Miao, T.; Wen, W.; Li, Y.; Wu, S.; Zhu, C.; Guo, X. Label3DMaize: Toolkit for 3D Point Cloud Data Annotation of Maize Shoots. *GigaScience* **2021**, *10*, giab031. [[CrossRef](#)] [[PubMed](#)]

Disclaimer/Publisher’s Note: The statements, opinions and data contained in all publications are solely those of the individual author(s) and contributor(s) and not of MDPI and/or the editor(s). MDPI and/or the editor(s) disclaim responsibility for any injury to people or property resulting from any ideas, methods, instructions or products referred to in the content.